

## X-RAY OBSERVATIONS OF SN 1006 WITH *INTEGRAL*

E. KALEMCI<sup>1,2</sup>, S. P. REYNOLDS<sup>3</sup>, S. E. BOGGS<sup>1,4</sup>, N. LUND<sup>5</sup>, J. CHENEVEZ<sup>5</sup>, M. RENAUD<sup>6,7</sup>, J. RHO<sup>8</sup>

*Accepted for publication in the Astrophysical Journal*

### ABSTRACT

The remnant of the supernova of 1006 AD, the remnant first showing evidence for the presence of X-ray synchrotron emission from shock-accelerated electrons, was observed for  $\sim 1000$  ksec with *INTEGRAL* for the study of electron acceleration to very high energies. The aim of the observation was to characterize the synchrotron emission, and attempt to detect non-thermal bremsstrahlung, using the combination of IBIS and JEM-X spatial and spectral coverage. The source was detected with JEM-X between 2.4 and 8.4 keV bands, and not detected with either ISGRI or SPI above 20 keV. The ISGRI upper limit is about a factor of four above current model predictions, but confirms the presence of steepening in the power-law extrapolated from lower energies ( $< 4$  keV).

*Subject headings:* ISM:individual (SN1006), supernova remnants, X-rays:observations, radiation mechanisms:non-thermal

### 1. INTRODUCTION

Supernova remnants (SNRs) have long been thought to be the primary site of Galactic cosmic ray acceleration up to the “knee” feature in the integrated cosmic-ray spectrum near 3000 TeV, as the supernova shocks are one of the few mechanisms that could provide enough energy to support this population (Dyer et al. 2001). However, many features of the acceleration process, including injection physics, efficiency, and maximum electron and ion energies, are not yet clear. Hard X-ray observations (above 10 keV) of SNRs may cast light on this poorly understood process.

High energy electrons in SNRs produce X-rays via two mechanisms, non-thermal bremsstrahlung and synchrotron radiation. Electrons can also produce gamma-rays up to TeV energies by inverse Compton (IC) scattering of any photons present, such as the cosmic microwave-background (CMB). In addition, relativistic protons can produce gamma-rays from the decay of  $\pi^0$  particles from inelastic ion-ion collision. All these processes have been extensively modeled for SNRs by various groups (Sturmer et al. 1997; Gaisser, Protheroe & Stanev 1998; Baring et al. 1999). In hard X-rays, synchrotron radiation from the tail of the electron distribution may compete with non-thermal bremsstrahlung from the very lowest-energy accelerated electrons.

SN 1006 has been the prototype laboratory for the study of electron acceleration to high energies in shocks. X-rays from this object were first reported by Winkler & Laird (1976). The earlier featureless spectrum (Becker et al. 1980) was modeled as the loss-steepened extrapolation of the radio synchrotron spectrum by Reynolds & Chevalier (1981). Later,

observations by *ASCA* (Koyama et al. 1995) showed that the limbs have featureless spectra well described by power-laws, whereas the interior has a thermal, line-dominated spectrum. The source was also observed with *RXTE*, and Dyer et al. (2001) showed that elaborate synchrotron emission models (Reynolds 1996, 1998) fit the combined *RXTE* - *ASCA* spectrum reasonably well.

Electrons producing keV synchrotron emission could also produce very high-energy photons (in the TeV range) by IC upscattering of CMB photons (Pohl 1996). The TeV flux depends on the electron distribution, and in conjunction with the synchrotron flux, a mean magnetic field strength of the remnant can be deduced. A detection of the northeast (NE) limb of SN 1006 was reported in ground-based TeV observations by *CANGAROO-I* (Tanimori et al. 1998). It is interesting that only one limb was detected, even though the X-ray spectra of the two limbs are similar (Allen, Petre & Gotthelf 2001; Dyer, Reynolds & Borkowski 2004). To have a discrepancy in the TeV band, the electron spectra, magnetic field strengths, or synchrotron and IC emission-angle distributions of the two rims would have to be different (Allen, Petre & Gotthelf 2001), but in a way that does not produce significant differences in the X-ray band.

The nature of X-ray emission from SN 1006 above 10 keV is still uncertain. Below 10 keV, synchrotron emission is the most plausible explanation. For synchrotron radiation, the quantitative inferences apply only to the exponential cutoff of the electron distribution. On the other hand, most of the accelerated electrons and much of their total energy reside in the lowest energy non-thermal electrons, whose bremsstrahlung emission could become dominant above 30 keV. In principle, the *INTEGRAL* observatory can examine the effects of both the lowest and highest energy non-thermal electrons by distinguishing the synchrotron and bremsstrahlung emission with its imaging and spectral capabilities.

Reynolds (1999) modeled bremsstrahlung and synchrotron emission from SN 1006. Synchrotron hard X-rays should be concentrated in two bright opposing limbs like the radio emission, and should dominate the emission below 30 keV. The images and spectra taken with *ASCA* (Koyama et al. 1995), *Chandra X-ray Observatory* (Long et al. 2003), and *XMM-Newton* (Rothenflug et al. 2004) confirm this below 10 keV. The non-thermal bremsstrahlung, resulting from slightly

<sup>1</sup> Space Sciences Laboratory, 7 Gauss Way, University of California, Berkeley, CA, 94720-7450, USA.

<sup>2</sup> Sabancı University, Orhanlı-Tuzla 34956, İstanbul, Turkey.

<sup>3</sup> Department of Physics, NC State University, 2700 Stinson Drive, Box 8202, Raleigh, NC 27695, USA.

<sup>4</sup> Department of Physics, University of California, 366 Le Conte Hall, Berkeley, CA, 94720-7300, USA.

<sup>5</sup> Danish National Space Center, Juliane Maries Vej 30, DK-2100 Copenhagen Ø, Denmark.

<sup>6</sup> Service d’Astrophysique, CEA-Saclay, 91191, Gif-Sur-Yvette, France

<sup>7</sup> APC-UMR 7164, 11 place M. Berthelot, 75231 Paris, France

<sup>8</sup> SIRTf Science Center, California Institute of Technology Mail Stop 220-6, Pasadena, CA 91125

supra-thermal shock-accelerated electrons interacting with thermal ions, is likely to be more symmetrically distributed, and will dominate at some energy between 30 and 300 keV. The bremsstrahlung flux will scale with the product of the thermal gas density  $n_{\text{th}}$  and the relativistic-electron density  $n_{\text{e,rel}}$ . The former can be constrained by observations of thermal X-ray emission, while the latter can be deduced from radio synchrotron fluxes if the magnetic field is known.

The TeV spectrum reported from *CANGAROO-I* (Tanimori et al. 1998) could be well-described by IC upscattered CMB photons, using a power-law electron spectrum with an exponential cutoff as described in Dyer et al. (2001). This fit gave a post-shock magnetic field of about 10  $\mu\text{G}$ . However, this result is now called into question by the observations of *H.E.S.S.*, which did not detect the source despite better sensitivity compared to *CANGAROO-I*. The TeV upper limits from *H.E.S.S.* are about a factor of 10 below the *CANGAROO-I* results<sup>9</sup> (Aharonian et al. 2005). These limits constrain IC upscattering of CMB photons by the same electrons that produce X-ray synchrotron emission: tighter limits mean fewer electrons, a higher magnetic field (Aharonian et al. place a lower limit of 25  $\mu\text{G}$  on the post-shock magnetic field), and less non-thermal bremsstrahlung. Lowering the possible IC-CMB flux by a factor of 10 directly lowers the allowable relativistic-electron density by the same factor, and hence lowers the predicted bremsstrahlung flux by an order of magnitude.

Even if bremsstrahlung is not detected, the detailed shape of the steepening synchrotron spectrum can provide information on the physical process causing the cutoff in the electron spectrum. This is crucial information for understanding the acceleration of cosmic rays, since if the cutoff is due to radiative losses on electrons, the proton spectrum might extend to much higher energies, perhaps as high as the knee. However, if the finite remnant age (or size) or some change in diffusive properties of the upstream medium causes the cutoff, it should also cut the proton spectrum off at a similar energy (between 10 and 100 TeV; Dyer et al. 2001), far below the “knee” energy. Detailed models show subtle but potentially distinguishable differences in the shape of the synchrotron spectrum above 10 keV, with loss-limited spectra (due to higher magnetic fields) being somewhat harder.

Our group has observed SN 1006 for  $\sim 1000$  ks with the *INTEGRAL* Observatory (Winkler et al. 2003) in AO-1 with the main aim of detecting and characterizing synchrotron emission, and distinguishing synchrotron and non-thermal bremsstrahlung emission by comparing the IBIS/ISGRI and JEM-X images to the model images. In this work, we will discuss the results of the analysis of the *INTEGRAL* data, and place limits on the synchrotron and bremsstrahlung emission from SN 1006.

## 2. OBSERVATIONS AND ANALYSIS

The *INTEGRAL* observations took place in two sets. The  $\sim 250$  ks first set (“Set I”) was conducted early in the mission, between Jan, 11, 2003, and Jan, 20, 2003, corresponding to *INTEGRAL* revolutions 30 and 32. The  $\sim 750$  ks second set (“Set II”) was conducted between Jan, 20, 2004 and Jan, 30, 2004, during revolutions 155-158. These two sets have different observational characteristics for different instruments as explained below, and only the data from Set II are used for

<sup>9</sup> Recent measurements by *CANGAROO-III* has also claimed null result on SN 1006 (Tanimori et al. 2005).

this paper. We did not use SPI (Spectrometer on *INTEGRAL*, Vedrenne et al. 2003), as ISGRI (see § 2.2 for more information) places much stricter limits in the hard X-ray band. Before the general analysis for all instruments, we filtered out the pointings with high Anti-Coincidence Shield rates, mostly occurring during the entry and exit of the radiation belts.

### 2.1. The JEM-X analysis

The Joint European X-ray Monitor, JEM-X, consists of two identical high pressure imaging micro-strip gas chambers, and makes observations simultaneously with the main instruments on *INTEGRAL*, albeit with a narrower fully-coded field of view of  $4.8^\circ$ . The energy band is 3–35 keV and the angular resolution is  $3.35'$  (Lund et al. 2003). Due to a problem with eroding anodes, the high voltage in the JEM-X detectors was lowered, and a new background rejection criterion was implemented after the launch. One of the detector pair is being kept in a safe state, and during our observations only JEM-X 2 was operational.

Set I was conducted before the new background rejection criteria were implemented in JEM-X, and therefore was not included in this analysis. We note that, although the total exposure for Set II is  $\sim 750$  ks, the effective exposure time of the central object is approximately 250 ks due to the vignetting of the JEM-X instrument during the 25 point dither. We have obtained JEM-X images in 4 energy bands using the *JEM-X Midispy offline software package* available from the DNSC (Lund et al. 2004). These energy bands<sup>10</sup> are 2.4–4.2 keV, 4.2–8.4 keV, 8.4–14 keV, and 14–35 keV. The images from each pointing are then mosaicked using the *mosaic-weight* program (Chenevez et al. 2004).

The fluxes and the significance values shown in Table 1 are derived using the inner ASCA contours enclosing the NE and SW limbs to define two shape templates. The NE template is constructed with 23 pixels inside the inner ASCA contour seen in Fig. 1 on the left. The SW template is also constructed similarly, using the 19 pixels inside the inner ASCA contour on the right. The count excesses in the JEM-X mosaic images are then determined inside these two regions. The relevant noise figures are derived by defining a number of non-overlapping regions with the reference templates within a  $60 \times 60$  pixel field ( $90 \times 90$  arcminutes) centered on SN1006. 114 NE-templates, each containing 23 pixels, can be arranged within the  $60 \times 60$  field. For the SW-template the corresponding numbers are 112 regions, each with 19 pixels. The statistical properties of the excess counts in these two sets of regions are used to derive RMS-noise of the background for regions of the two shapes. The signal-to-noise ratio derived in this way will obey normal statistics because the region templates are defined independently of the JEM-X data.

The fluxes are derived by comparing the excesses in the SN 1006 mosaics with corresponding excesses in mosaic images of the Crab Nebula obtained with the same *INTEGRAL* dither pattern, and correcting for the difference in the effective observation time.

### 2.2. The ISGRI analysis

One of the two main instruments on *INTEGRAL*, IBIS (Imager on Board the *INTEGRAL* Satellite, Ubertini et al. 2003), consists of two cameras. The *INTEGRAL* Soft Gamma-ray

<sup>10</sup> The low energy threshold is variable over different parts of the JEM-X detector.

Imager, ISGRI, is the low-energy camera of the IBIS telescope (Lebrun et al. 2003). It has a large sensitive area of  $2621 \text{ cm}^2$  made up of 16384 CdTe pixels. The angular resolution is  $\sim 13'$  (Gros et al. 2003), and the fully-coded field of view is  $9^\circ$ . The energy range is 20 keV – 10 MeV. The older background maps for Set I observations resulted in much noisier images compared to Set II images, and therefore we limit the analysis to the data from Set II. We used OSA 4.2 (Goldwurm et al. 2003) standard programs to obtain images in 20–40 keV and 40–100 keV bands.

Since the ISGRI system point spread function is  $\sim 13'$ , SN 1006 ( $\sim 30'$  diameter) appears as an extended object to the imager. Estimation of the flux of such sources with a coded-mask instrument is complicated, since the mask patterns used in gamma-ray astronomy are optimized for point sources. One needs to use simulations to obtain the effect of the extended nature of the source on the image and the measured flux. Such simulations have been conducted for ISGRI for different extended source geometries, including SN 1006 (Renaud et al. 2005). For SN 1006, Renaud et al. (2005) used an input image of the expected synchrotron emission map in 20–40 keV band based on the simulations described in Reynolds (1999). The principle of the ISGRI simulations is the following: For each point-like source constituting the extended one, the corresponding shadowgram (the image of the mask pattern illuminated and projected onto ISGRI) is calculated. The final expected shadowgram of SN 1006 is obtained by summing all these contributions. Then, the standard deconvolution (see Goldwurm et al. 2003, for details) in OSA is applied to obtain the reconstructed image. With this technique, Renaud et al. (2005) obtained a reduction factor of 0.7: that is, ISGRI would detect 70% of the true flux at each limb.

### 3. RESULTS

#### 3.1. JEM-X results

The source is detected at the limbs in 2.4–4.2 keV and 4.2–8.4 keV bands (see Fig. 1 and Table 1). **This is the first time that the structure of an individual extended source has been imaged with *INTEGRAL*.** It appears that the South-West (SW) limb (the limb on the right in the images) is stronger in the 2.4–4.2 keV band at about the  $1\sigma$  level, but the trend is reversed at higher energies. At 4.2–8.4 keV, the NE limb is stronger, a result with higher significance. An excess at the position of the NE limb is present in the 8.4–14 keV band ( $1.7\sigma$ ), but no excess is seen in the SW limb. We note that *XMM-Newton* data also points to an asymmetry in flux coming from the NE and SW limbs such that the NE limb gets relatively stronger as energy increases (Rothenflug et al. 2004). A similar trend is seen in *ASCA* data (Dyer, Reynolds & Borkowski 2004), but the differences are small in the *ASCA* band (below 8 keV). The small excess of the SW over NE limbs in the 2.4–4.2 keV band we see is not supported by *ASCA* or *XMM-Newton* observations in that energy range.

Figure 2 shows our combined JEM-X fluxes for both limbs, compared with previous spatially integrated pre-*ASCA* flux measurements (see Reynolds 1996; Hamilton, Sarazin & Szymkowiak 1986 for references). The integrated fluxes have been converted to flux densities assuming a photon index  $\Gamma$  of 3.0 (Allen, Petre & Gotthelf 2001). Also shown are a pair of model curves for the escape model that provided a good fit to *ASCA* and *RXTE* data in Dyer, Reynolds & Borkowski (2004). The parameters of the

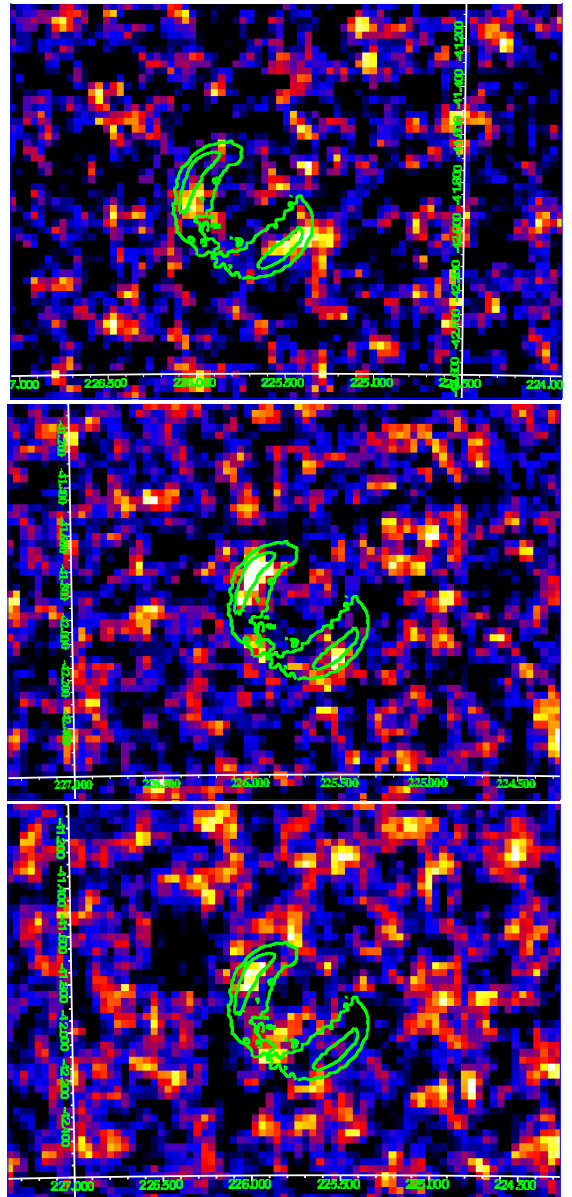


FIG. 1.— JEM-X reconstructed images of SN 1006 in three energy bands. Top: 2.4–4.2 keV, middle: 4.2–8.4 keV band, bottom: 8.4–14 keV. The *ASCA* contours are overlaid. The detection significances, fluxes, and upper limit fluxes are shown in Table 1. (The electronic version has this figure in color.)

best fit are a roll-off frequency of  $\nu_{\text{roll}} = 3.0 \times 10^{17} \text{ Hz}$  and an electron energy index of 2.2 (implying a radio spectral index  $\alpha = 0.6$  or radio photon index  $\Gamma \equiv \alpha + 1 = 1.6$ ). These parameters imply an e-folding energy of the exponential cutoff (due to escape) of  $32(B_2/10\mu\text{Gauss})^{-1/2} \text{ TeV}$  (where  $B_2$  is the post-shock field). The curves in Figure 2 correspond to  $\pm 1\sigma$  errors on  $\nu_{\text{roll}}$ :  $(2.8 - 3.1) \times 10^{17} \text{ Hz}$ . The dashed line indicates the bremsstrahlung prediction for an upstream density of  $0.2 \text{ cm}^{-3}$  and  $B_2 = 10\mu\text{Gauss}$ .

#### 3.2. ISGRI results

We obtained ISGRI images in different energy bands using OSA 4.2. SN 1006 was not detected in any band. The 20–40 keV sigma image is shown in Fig. 3. The  $3\sigma$  upper limit (sensitivity limit) for a point source for  $\sim 750 \text{ ks}$  observing time is  $\sim 9 \times 10^{-5} \text{ photon cm}^{-2} \text{ s}^{-1}$ . If synchrotron dominates

TABLE 1  
JEM-X SUMMARY

<b>North-East Limb</b>			
Energy band (keV)	Flux ( $10^{-4}$ photon/cm <sup>2</sup> s)	Statistical significance	Model flux <sup>a</sup> ( $10^{-4}$ photon/cm <sup>2</sup> s)
2.4–4.2 <sup>b</sup>	$10 \pm 4$	2.6	14
4.2–8.4	$11 \pm 2$	5.0	5.9
8.4–14	$3.3 \pm 1.9$	1.7	1.4
<b>South-West Limb</b>			
2.4–4.2	$15 \pm 4$	4.0	13
4.2–8.4	$3.6 \pm 2.3$	1.6	4.8
8.4–14	$<5.7$	3 <sup>c</sup>	-

<sup>a</sup>Flux from extrapolated model fit to the *ASCA* spectrum (0.8 - 9 keV), Dyer, Reynolds & Borkowski 2004

<sup>b</sup>The actual low energy threshold is variable over different parts of the JEM-X detector.

<sup>c</sup> $3\sigma$  upper limit

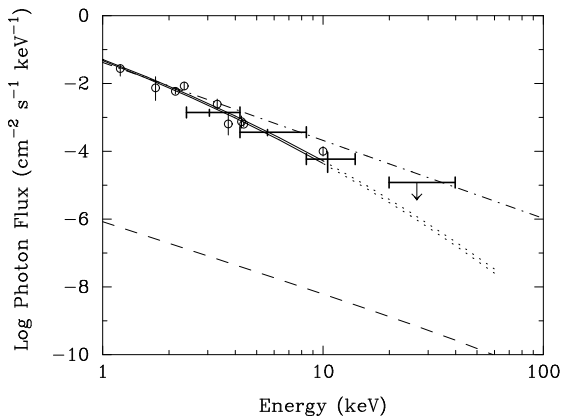


FIG. 2.— Integrated hard X-ray spectrum of SN 1006. The heavy bars show the energy bins over which our JEM-X fluxes are integrated. The integrated fluxes were converted to spectral fluxes assuming a power-law index of 3.0, and plotted at the median energy of each bin. The errors in the bin energies are insignificant (much smaller than the line widths). The upper limit bar is from ISGRI. Open circles are pre-*ASCA* (see text) observations, and the two solid lines are the  $\pm 1\sigma$  model fits to *ASCA* and *RXTE* data, extrapolated to the higher energies (Dyer et al. 2001). The dotted-and-dashed line is the extrapolation from the *Chandra* spectral fit (Long et al. 2003). The dashed line is the bremsstrahlung prediction of the model described in text.

in 20–40 keV band, the emission would be concentrated in two limbs. The extended nature of the source causes a reduction factor of 0.7 in flux (see § 2.2). Therefore the  $3\sigma$  upper limit for a synchrotron dominated source is  $1.3 \times 10^{-4}$  photon  $\text{cm}^{-2} \text{s}^{-1}$  at each limb. For synchrotron dominated emission, the expected total flux in the 20–40 keV band (based on the models shown in Figure 2) is  $(2.9 - 3.6) \times 10^{-5}$  photon  $\text{cm}^{-2} \text{s}^{-1}$  for the entire remnant, or roughly half this at each limb. The bremsstrahlung emission from the model shown in Figure 2, using the lower-limit  $25 \mu\text{G}$  downstream magnetic field from *H.E.S.S.* TeV observations, is predicted to be about  $2 \times 10^{-8}$  photon  $\text{cm}^{-2} \text{s}^{-1}$ , far below ISGRI’s sensitivity. In fact, in this case, since the emission would be coming from a larger area, the upper limit set by our observations is even higher. The predicted crossover energy where bremsstrahlung and synchrotron emission become comparable is in the vicinity of 200 keV.

Long et al. (2003) reported that a power-law photon index of 2.30 fit the *Chandra* data well between 0.5 and 5 keV for the emission at the limbs. An extrapolation of this fit from 5

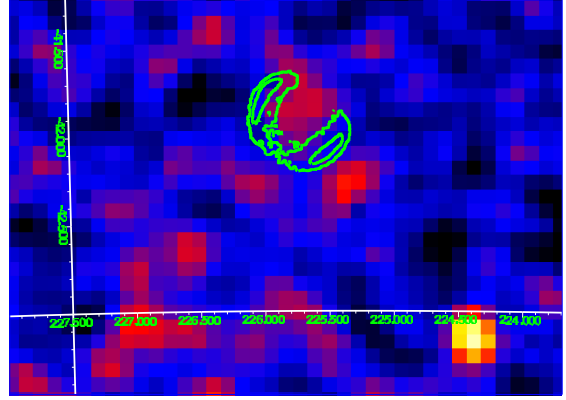


FIG. 3.— The ISGRI sigma image around SN 1006 in 20–40 keV band. SN 1006 is not detected. A nearby source (possibly VV 780,  $11.6\sigma$  detection Kalemci, Boggs & Lund 2005) is also shown for comparison. The *ASCA* contours are overlaid to show the expected position of SN 1006. The feature at the center of SN 1006 is not significant, and is possibly due to inaccurate background map. (The electronic version has this figure in color.)

keV to the ISGRI range is also shown in Fig. 2 with a dotted-and-dashed line. Our ISGRI upper limit is about a factor of 2 below the extrapolation of this power-law to 28 keV.

#### 4. DISCUSSION

Coded-mask imaging is a complex process, and optimal techniques are still being developed to clean noisy images, both for JEM-X and ISGRI. Our results confirm and extend results obtained with *ASCA*, *Chandra X-ray Observatory*, and *XMM-Newton*, and show that relatively small increases in sensitivity may allow ISGRI to detect predicted synchrotron radiation for some models.

The prospect of detecting bremsstrahlung X-rays or gamma-rays from SN 1006 has become considerably more remote with the combination of lower estimates for the ambient density and the much higher magnetic field that would be required to explain the lack of IC from CMB photons in the *H.E.S.S.* observations. However, it is quite possible that a somewhat longer *INTEGRAL* observation scheduled for Cycle 3 will have sufficient sensitivity to detect synchrotron emission in the 18–40 keV band. A model that can describe the observations of Figure 2 but with a strong enough magnetic field to satisfy the *H.E.S.S.* constraints (downstream  $B > 25 \mu\text{G}$ ) is somewhat harder than the spectra shown in Figure 2, and predicts a flux in the 18–40 keV band of  $0.3 \times 10^{-4}$  photon  $\text{cm}^{-2} \text{s}^{-1}$ . Some models predict considerably lower fluxes in the 18–40 keV band, so ISGRI detection would not only extend and confirm the presence of hard synchrotron X-rays, but could provide useful model discrimination.

We have obtained the first observations with JEM-X of an extended source, between 2.4 and 14 keV. The fluxes we derive are consistent with those of earlier imaging observations where they overlap, and support the identification of the continuum emission of SN 1006 as synchrotron radiation from a slowly dropping off electron distribution. Our ISGRI  $3\sigma$  upper limit is about a factor of 4 higher than the prediction of the model that best fits the soft X-ray continuum. With ISGRI, we confirm at higher energies than has been previously reported that the X-ray spectrum of SN 1006 must be steepening. A somewhat longer observation, and more developed data analysis techniques, should allow the detection of SN 1006 in the 18–40 keV band with ISGRI, and above 8.4 keV with JEM-X,

and can provide important modeling constraints.

E.K. is supported by the European Commission through a FP6 Marie-Curie International Reintegration Grant (IN-

DAM). E.K. acknowledges partial support of TÜBİTAK. E.K. and S.E.B. acknowledge NASA grants NAG5-13142 and NAG5-13093. S.P.R. acknowledges support from NASA grant NAG5-13092.

#### REFERENCES

- Aharonian, F., et al., 2005, *A&A*, 437, 135  
 Allen, G. E., Petre, R., & Gotthelf, E. V., 2001, *ApJ*, 558, 739  
 Baring, M. G., Ellison, D. C., Reynolds, S. P., Grenier, I. A., & Goret, P., 1999, *ApJ*, 513, 311  
 Becker, R. H., Szymkowiak, A. E., Boldt, E. A., Holt, S. S., & Serlemitsos, P. J., 1980, *ApJ*, 240, L33  
 Chenevez, J., Lund, N., Westergaard, N. J., Budtz-Joergensen, C., Kretschmar, P., & Walter, R., 2004, to appear in: Proc. of The 5th INTEGRAL Workshop, The INTEGRAL Universe, Munich, 16-20 Feb. 2004, astro-ph/0406682  
 Dyer, K. K., Reynolds, S. P., & Borkowski, K. J., 2004, *ApJ*, 600, 752  
 Dyer, K. K., Reynolds, S. P., Borkowski, K. J., Allen, G. E., & Petre, R., 2001, *ApJ*, 551, 439  
 Gaisser, T. K., Protheroe, R. J., & Stanev, T., 1998, *ApJ*, 492, 219  
 Goldwurm, A., et al., 2003, *A&A*, 411, L223  
 Gros, A., Goldwurm, A., Cadolle-Bel, M., Goldoni, P., Rodriguez, J., Foschini, L., Del Santo, M., & Blay, P., 2003, *A&A*, 411, L179  
 Hamilton, A. J. S., Sarazin, C. L., & Szymkowiak, A. E., 1986, *ApJ*, 300, 698  
 Kalemci, E., Boggs, S. E., & Lund, N., 2005, *The Astronomer's Telegram*, 410  
 Koyama, K., Petre, R., Gotthelf, E. V., Hwang, U., Matsuura, M., Ozaki, M., & Holt, S. S., 1995, *Nature*, 378, 255  
 Lebrun, F., et al., 2003, *A&A*, 411, L141  
 Long, K. S., Reynolds, S. P., Raymond, J. C., Winkler, P. F., Dyer, K. K., & Petre, R., 2003, *ApJ*, 586, 1162  
 Lund, N., et al., 2003, *A&A*, 411, L231  
 Lund, N., et al., 2004, in Proc. of The 5th INTEGRAL Workshop, The INTEGRAL Universe, Munich, 16-20 Feb. 2004  
 Pohl, M., 1996, *A&A*, 307, L57  
 Renaud, M., Lebrun, F., Terrier, R., Reynolds, S. P., & Kalemci, E., 2005, submitted to *A & A*  
 Reynolds, S. P., 1996, *ApJ*, 459, L13  
 Reynolds, S. P., 1998, *ApJ*, 493, 375  
 Reynolds, S. P., 1999, *Astrophys. Lett. Commun.*, 38, 425  
 Reynolds, S. P., & Chevalier, R. A., 1981, *ApJ*, 245, 912  
 Rothenflug, R., Ballet, J., Dubner, G., Giacani, E., Decourchelle, A., & Ferrando, P., 2004, *A&A*, 425, 121  
 Sturmer, S. J., Skibo, J. G., Dermer, C. D., & Mattox, J. R., 1997, *ApJ*, 490, 619  
 Tanimori, T., et al., 1998, *ApJ*, 497, L25-L28  
 Tanimori, T., et al., 2005, Proceedings of the 29th International Cosmic Ray Conference, August 03-10, 2005, Pune, India, 101  
 Ubertini, P., et al., 2003, *A&A*, 411, L131  
 Vedrenne, G., et al., 2003, *A&A*, 411, L63  
 Winkler, C., et al., 2003, *A&A*, 411, L1  
 Winkler, P. F., & Laird, F. N., 1976, *ApJ*, 204, L111